Article

A Design Procedure for Anchors of Floating Ocean Current Turbines on Weak Rock

Francisco Bañuelos-García [1,*], Michael Ring [2], Edgar Mendoza [2] and Rodolfo Silva [2]

1 Facultad de Ingeniería, Universidad Autónoma del Estado de México, Cerro de Coatepec S/N, Ciudad Universitaria, Toluca 50110, Mexico

2 Instituto de Ingeniería, Universidad Nacional Autónoma de México, Coyoacán 04510, Mexico; mring@iingen.unam.mx (M.R.); emendozab@iingen.unam.mx (E.M.); rsilvac@iingen.unam.mx (R.S.)

* Correspondence: hbanuelosg589@profesor.uaemex.mx

Abstract: In recent years, ocean current turbines have proven to be a reliable device for renewable energy generation. A crucial element of these turbines are the foundations, since they limit the displacement of the turbine, which is key in achieving efficiency in energy conversion, and can account for up to 26% of the total cost of the project. Most design procedures for foundations focus on sandy and clayey soils, but rock soils often predominate in tropical locations where marine currents are suitable for the installation of this type of turbine. This paper presents a design procedure for steel pile anchors (PAs) and concrete dead weight anchors (DWAs) on weak rock soils, using the assumptions of current technical documents and design codes commonly used in the industry for marine structures. Using specific designs for PA and DWA anchors, the procedure was theoretically assessed for a site off Cozumel Island, Mexico. The results show that the dimensions needed for DWAs are substantially larger than those for PAs. Therefore, whenever drilling is economically and operatively possible, piles would be preferable for the foundations of current turbine systems.

Keywords: ocean current turbine; foundation design; dead weight anchor; pile anchor; limestone seabed; design procedure

1. Introduction

In the present search for more sustainable forms of energy, ocean currents offer a significant and relatively predictable source of power, for conversion into electricity. Ocean currents have approximately seven times the energy density of wind currents. However, as they are installed in a more demanding environment, biophysically, these technologies are less developed. Turbines capable of exploiting those currents are usually submerged structures, and so are a more attractive alternative in locations where aesthetics, hurricane risk and navigation are a constraint. To attain maximum efficiency, these turbines require an adequate foundation; otherwise, displacement may occur, resulting in malfunction, or even the loss of the device. An informed choice of foundation is important, since it accounts for 10–26% of the total cost of a project [1,2].

An ocean current turbine can be a fixed, or floating, device. The first is a rigid or semi-rigid structure, which does not move from its installation site. This system does not require any additional elements connected to the turbine and is suitable in shallow depths of 20 to 60 m [3,4]. The installation of this type of foundation can be expensive and its maintenance may be unaffordable [5]. To overcome these shortcomings, floating systems have been developed, consisting of a turbine on a floating platform which is fastened to an anchor by means of synthetic ropes, cables, or chains. The main advantage of floating systems is that they can be installed in depths greater than 60 m [3].

The anchors that are in floating systems of marine current turbines are fluke, pile, deadweight, and plate structures (see Figure 1). Fluke (or drag embedded) anchors are installed by pulling on the anchor line and dragging it along the sea floor. Eventually, the

fluke will penetrate the sea floor and the anchor will be embedded. Pile anchors (PA) are installed either by hammering them into the ground, or by drilling and grouting them in place, depending on the nature of the sea floor. Specific designs for marine rock anchors have been presented by various companies. Marine Micropile Technology Ltd. (Dublin, Ireland) developed drilled and grouted pile anchors for use in offshore projects to reduce the cost for foundations [6], based on the technology used at onshore construction sites. The installation uses a simultaneous drilling and grouting process, made possible by a special pile tip that serves as both a drill bit and a nozzle for the grout. Another proprietary rock anchor is presented in [7], in which the anchor and the drill bit are present in the same unit. After installing the anchor in the rock, parts of it are expanded and pressed against the bore hole by tensioning specific parts of the anchor. Both of these methods are well developed at present, but very little information is given as to the underlying calculations and design choices required in the earlier stages of a project. On the other hand, deadweight anchors (DWAs) are simply placed on the sea floor and hold the turbine in place by their sheer weight and friction with the sea floor. Plate anchors can be installed using various methods, all requiring a metal rod or tube to push the anchor to the desired depth below the seabed and then rotate them to their final orientation [8].

(a)　　　　　　**(b)**　　　　　　**(c)**　　　　　　**(d)**
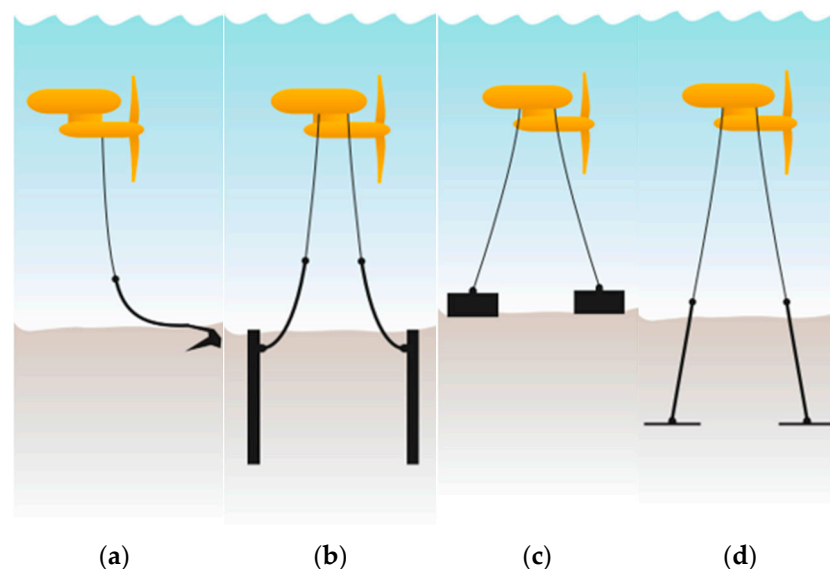
Figure 1. Types of foundations for ocean current turbine anchorage. (**a**) Fluke; (**b**) Pile; (**c**) Deadweight; (**d**) Plate.

The most relevant aspects to be considered in selecting an anchor type are:

- Local water depth;
- Type of seabed;
- Installation complexity;
- Characteristics of the turbine;
- Transportation of the system components.

Although initially the factor deciding the foundation type is the water depth, the soil properties are the most important element to consider [4]. Depending on the type of sea floor; fluke or plate anchors would be very complicated, even unfeasible, on a rocky seabed [8].

In Mexico, the most suitable site for the installation of an electric power generation plant based on ocean current turbines is off Cozumel Island in the Mexican Caribbean [9]. The current there is part of the ocean and wind-driven circulation system and so is persistent all year round in direction and magnitude. Recent studies show the hydrokinetic energy at this location offers great potential, both in shallow and deep water [10,11]. Unlike the sea floor in most parts of the world, the seabed of the Mexican Caribbean is predominantly

limestone, covered with a thin layer of finer sediment [12], something relatively common in tropical and subtropical zones. The most suitable anchors for this type of soil are deadweight (DWA) and pile anchors (PA).

While design methods for anchorage in clay and sandy soils are widely available [8], there are fewer generic design procedures for DWAs and PAs for offshore structures. Taylor [13] proposed a practical, up-to-date guide that enables an engineer to select the type and size of anchor needed, including direct-embedment anchors, DWAs, and drag-embedment anchors. Based on this work, VanZwieten et al. [14] proposed a preliminary design process for estimating the geometry and required weight of the anchor. These parameters are calculated using the components of the design forces, and the specific weight of the material, which are not difficult to obtain. Technical documents such as: DNV-OS-J101 [15] and API RP2A-WSD [16] are also available, which give guidelines for design. In the case of PAs, various design procedures have been developed for offshore structures [3,17–22], and there are technical design documents for these foundations, such as API RP 2A-LRFD [16] and DNV-OS-J101 [15]. The design procedures are comprehensive, proven, and almost identical, but they are only applicable for clayey and sandy soils. However, there are potential sites, such as Cozumel, where ocean current turbines are feasible and the predominant soil is mainly rocky.

Weak rock often has complex mechanical behavior, mostly dis-homogeneous and anisotropic, due to the presence of defects or pre-existing discontinuities [23], and is considered a mid-point between soil and hard rocky spoils. This means a specific design procedure is needed, which considers its geotechnical properties [24]. The behavior of weak rock is related to its secondary structure, that is, the spacing and thickness of the soil-filled cracks and joints, and its compressive strength [25]. Therefore, placing foundations on weak rock may result in greater displacements and deformations; specific calculation procedures are needed. There are various procedures for the design of PAs in weak rock; for example, Goodman [26], Abbs [27], Carter and Kulhawy [28], Gannon et al. [29], Zhang et al. [30], Irvine et al. [31]; but all of these are related to onshore structures. Therefore, existing design methods must be adapted, since anchors in or on rock behave significantly differently to anchors in or on sandy or clayey soils. Despite this, to the best of the authors' knowledge, there has been no research into the comprehensive design of ocean current turbine anchors on weak rock.

This paper presents a design procedure for ocean turbine foundations, using steel piles (PA) or concrete deadweight anchors (DWAs) on weak rock. It is based on the hypotheses of technical documents such as: API RP2A-WSD [16], DNV-OS-J101 [15], IEC 62600-10 [32], as well as the most commonly used procedures for the design of DWAs and PAs in weak rock [14,25–31,33].

The main dimensions of the anchor are determined without considering specific details, such as the connection between the pad eye and the anchor. The proposed methodology involves three main steps:

(i)   Determining the preliminary design of the anchor (geometry);
(ii) Evaluating the structural capacity of the anchor; and
(iii) Computing the geotechnical capacity of the anchor on rock.

From these results, the most appropriate anchor design is selected.

The application of the proposed procedure is applied to an ocean current turbine site in the Cozumel channel, Mexico. The article is organized as follows: In Section 2 the procedure proposed is presented, divided into ultimate states, services, and fatigue limit designs. Section 3 gives an application example, as well as design results, and Section 4 presents the conclusions of the work.

2. Proposed Design Procedure

In this section, a design procedure for DWA and PA on weak rock is presented, which can be extrapolated for anchoring systems. A flow chart of the design procedure is shown

in Figure 2. The procedure consists of satisfying the three limit states (see Figure 3) for the design of offshore foundations/anchors.
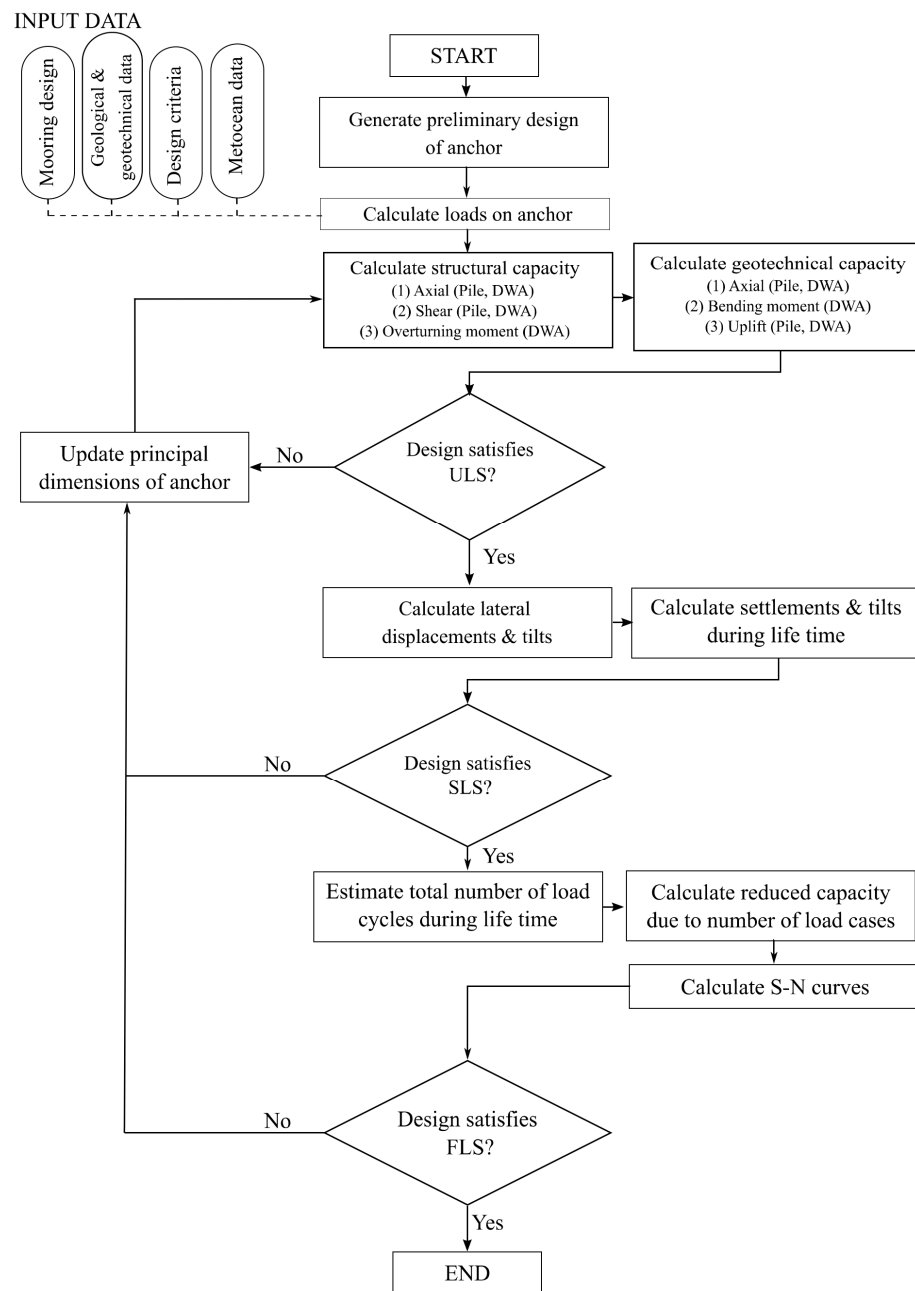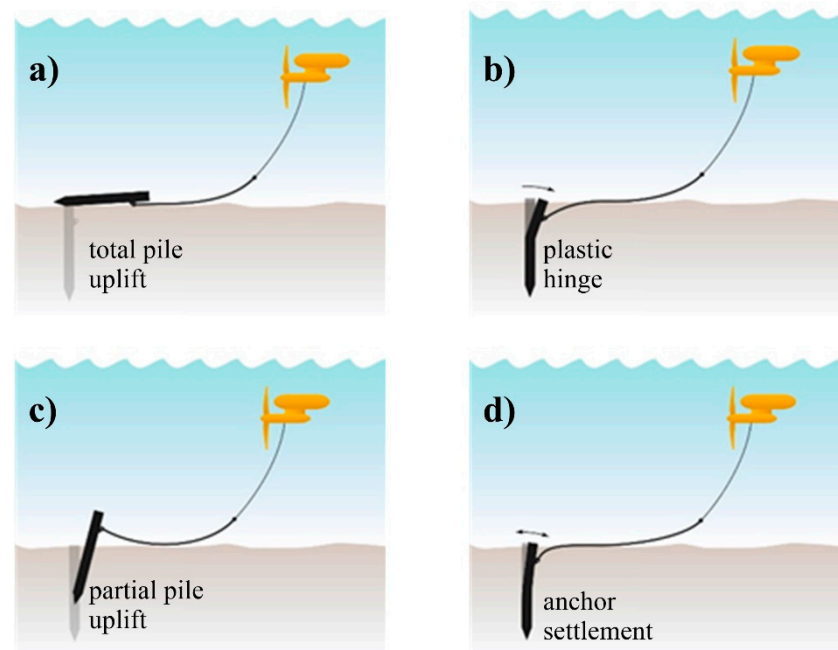

Figure 2. Flow chart of the proposed design procedure.

Figure 3. Examples of limit states of pile anchors for ocean current turbines, (**a**) ULS: total pile uplift; (**b**) ULS: formation of a plastic hinge in steel piles; (**c**) SLS: malfunction derived from a partial pile uplift; (**d**) SLS: security risk due to anchor settlement.

　　The limit states for the design of ocean current turbine anchors are very similar to those of wind turbines [3,17]. The ultimate limit state (ULS) corresponds to the failure of the anchor when its maximum load resistance is exceeded. This may occur due to factors such as:

- Static equilibrium of the anchor is lost (whole or part), with a consequent failure mechanism, such as overturning, sliding, uplift. The case of a total pile uplift is shown in Figure 3a.
- Structural resistance is lost, leading to excessive yielding and the formation of a plastic hinge or cracks in concrete elements. Figure 3b shows a steel pile with a plastic hinge.
- Component fracture (for example, in the connections).

　　The service limit state (SLS) corresponds to the tolerance criteria of the anchor response to environmental loads being exceeded. This could include:

- Excessive displacements or rotations, leading to total, or partial, malfunction of the turbine. In Figure 3c, the pile has not moved completely, but the device will no longer generate electricity.
- Excessive vibration, limiting the performance of non-structural components.
- Differential settlements of the anchor, generating excessive rotation of the system. In Figure 3d, the back-and-forth movement of the pile lessens the stability and safety of the turbine.

　　The fatigue limit state (FLS) corresponds to long-term cyclic stresses and strains, which lead to failure of the anchor. These may be derived from repetitive loads or dynamic actions (i.e., wave loads, low frequency currents) acting on the anchor during its lifetime.

　　The ULS design has three phases, the first, preliminary design uses practical Equations for ordinary structures, or the designer's experience. Secondly, the capacity of the pre-designed structure is evaluated. Then, in the third phase, the geotechnical capacity of the anchor on rock is evaluated. In the SLS design, if required, the displacements and rotations of the structure are determined and compared with the maximum values allowed, based on research, technical documents, and design codes. Finally, in the FLS design, the cumulative damage to the anchor, derived from repeated loads or dynamic actions using S–N curves,

DNV-RP-C203 [34] for steel structures, and DNV-OS-C502 [35] for concrete structures, is determined.

2.1. Ultimate Limit State Design

The ULS must be fulfilled in accordance with the recommendations of existing design codes and technical documents for this type of structure, for example, API, DNV/DNV GL, IEC. The structural capacity of the anchor in this type of soil governs the design, since rock is more resistant than sandy or clayey soils. Therefore, the design procedure starts with the structural capacity, followed by the geotechnical capacity.

2.1.1. Pile Anchors (PA)

Wind and ocean current turbines installed on fixed, or on floating platforms usually have pile foundations [3]. Compared to other types of foundations, such as DWAs, pile foundations have an important axial and lateral load capacity. However, pile foundations are usually deployed in clay and sandy soils, due to the difficulty of drilling rock.

Preliminary Design

1. Initial parameters. The environmental and structural data for the design is collected, these are specific parameters from the deployment site and device such as: characteristics of the ocean current turbine, geotechnical parameters, and environmental loads, such as marine currents. The mechanical properties of the steel are also needed; for example, yield stress, F_y, ultimate stress, F_u, Young's modulus, E_s. The latter can be obtained from the design codes and technical documents of steel structures API RP 2A-LRFD [16].
2. Structural analysis. Based on the loads obtained and using the procedures recommended in the specialized literature [3,14], the mechanical elements are obtained, namely: axial force, shear force, overturning moment, displacements and rotations.
3. Pre-dimensioning of the diameter. A preliminary pile diameter is proposed, based on the designer's experience or on practical recommendations.
4. Pile wall thickness. The thickness of the pile, t_P, is determined using the following Equation API RP2A-WSD [16]:

$$t_P = \left[6.35 + \frac{D_P}{100} \right] \tag{1}$$

   where D_P is the pile diameter in mm and t_P is the thickness of the pile wall in mm.
5. Embedded length. The embedded length, L_r, is computed with the formula of Poulos and Davis [36]:

$$L_r = 4 \left(\frac{E_s I_P}{n_h} \right)^{\frac{1}{5}} \tag{2}$$

   where L_r is the embedded length in m; E_s is Young's modulus of the steel, I_P, is the second moment of area (see Appendix A), and n_h is the horizontal coefficient of the subgrade reaction.

Structural Capacity

6. Axial capacity (structural). Anchors for floating structures are only loaded by tension stresses. The structural capacity to axial loads is determined, based on API RP 2A-LRFD [16]:

$$Q_{RASP} = \phi_{t,y} F_y A_p \tag{3}$$

   where F_y is the yield stress of the steel, A_p, is the cross-sectional of the anchor, and $\phi_{t,y}$ is the resistance factor for axial tensile strength, which can be taken as 0.95 API RP 2A-LRFD [16].

7. Lateral capacity (structural). The shear capacity, Q_{RLSP}, of the pile can be determined, using the following expressions [37]:

$$Q_{RLSP} = \frac{\phi_{vs} \, F_{cr} \, A_p}{2} \tag{4}$$

with

$$F_{cr} = max(F_{cr1}, F_{cr2}) \tag{5}$$

$$F_{cr1} = \frac{1.60 \, E_s}{\left(\frac{D_p}{t_p}\right)^{\frac{5}{4}} \sqrt{\frac{L_r}{D_p}}} \tag{6}$$

$$F_{cr2} = \frac{0.78 \, E_s}{\left(\frac{D_p}{t_p}\right)^{\frac{3}{2}}} \tag{7}$$

F_{cr} is the maximum value between Equations (6) and (7) and must not exceed $0.6 \, F_y$. The resistance factor for lateral strength, ϕ_{vs} is 0.90 LRFD [37].

8. Revision of structural capacity. To satisfy the design requirements, the total force on the mooring system (V_d, H_d) must not exceed the axial (Q_{RASP}) and lateral capacities (Q_{RLSP}). It is worth mentioning that buckling does not occur in anchors for floating. However, it can be estimated by the Equations presented in DNV-OS-J101 [15]. If the above requirements are not fulfilled, the pile geometry must be modified, and the revision procedure restarted.

Geotechnical Capacity

In this section, the geotechnical capacity of piles on rock is determined.

9. Resistance of the pile shaft. The ultimate shaft resistance, Q_f, can be calculated using the following expression:

$$Q_f = \sum_1^N f \, A_f \tag{8}$$

where f is the unit outside shaft friction and N is the number of layers.

(a) Cohesionless Soil Interface

For piles in cohesionless soils, Q_f can be calculated with Equation (9) API RP2A-WSD [16]:

$$Q_f = K \, p_0' \, tan(\mathsf{F}) A_f < f_l A_f, \tag{9}$$

where K is the coefficient of lateral earth pressure, p_0' is the effective overburden pressure, F is the friction angle between the soil and the pile wall, A_f is the surface area of the pile shaft (see Appendix A), and f_l is the limiting skin friction. Further information regarding the definition of K, and p_0' can be found in [38].

(b) Cohesive Soil Interface

For piles in cohesive soils, Q_f, is calculated using the following expression [16]:

$$Q_f = \alpha s_u A_f \tag{10}$$

where s_u is the undrained shear strength, and α is the adhesion factor. This factor is related to undrained shear strength, effective overburden pressure, and interface roughness [31].

(c) Chalk

The widely accepted guidance on pile design in chalk provided by CIRIA [29] suggests that the limiting skin friction varies between 30 kPa and 50 kPa for large- displacement,

pre-formed piles in low to medium density chalk [39] defined the peak post-cyclic shear strength, $f_{s,limit}$, as:

$$f_{s,limit} = \left[\frac{tan(\delta)}{tan(\phi')}\right] s_u \tag{11}$$

where δ is the steel-chalk interface friction coefficient, ϕ' is the post peak internal soil friction coefficient (from cyclic simple shear), and s_u is the undrained shear strength.

(d)   Rock Socket Interface

A significant amount of research has been undertaken regarding the pile-rock interface for rock socket piles. The roughness and cleanliness of the rock socket are important factors in determining the pile-rock adhesion and have a significant influence on pile load capacity. The limiting skin friction for grouted rock sockets is often governed by the rock strength as follows:

$$Q_f = \alpha q_u A_f \tag{12}$$

where α is the adhesion factor, which depends on socket roughness but is generally taken as 0.1 for a smooth socket [29].

10.   Geotechnical capacity. The axial geotechnical capacity, Q_{RAGP}, of piles driven into rock depends on the resistance of the pile shaft, Q_f, defined in Equations (8)–(12), and the submerged weight of the pile, W_p (see Appendix A), given in Equation (A1). Figure 4 shows free-body diagram of the pile anchor.

$$Q_{RAGP} = Q_f + W_p \tag{13}$$
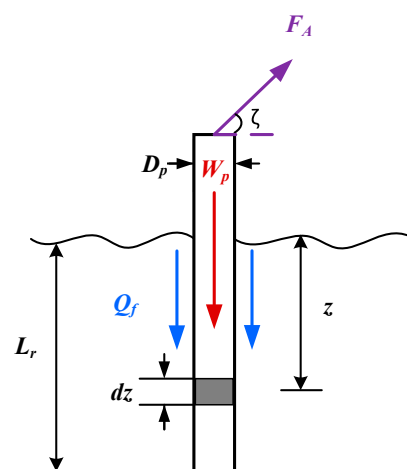
Figure 4. Free-body diagram of a pile anchor.

The lateral geotechnical capacity, Q_{RLGP}, is calculated using the so-called P–Y curves; for example, Carter et al. [28], Reese [25], Gabr et al. [40], and Zhang et al. [30] (see Appendix B).

11.   Geotechnical design revision. The acting design loads on the pile, (V_d, H_d), must not exceed the geotechnical capacity, (Q_{RAGP}, Q_{RLGP}). Otherwise, the diameter must be reviewed and adjusted accordingly, followed by a re-evaluation of the anchor, starting the design procedure, from Step 3.

2.1.2. Dead Weight Anchors

A dead weight anchor (DWA) is made of concrete, without steel reinforcement, and must have the necessary weight to bear the environmental demands and the action of the turbine. The advantages of this type of anchoring are that they do not requiring drilling; in

comparison with embedded anchors such piles, they can be built from materials commonly used for onshore structures and can be easily recovered from the installation site.

The design procedure for DWAs considers the so-called shear keys, which increase the lateral anchor holding capacity by inducing failure in the soil and not at the anchor soil interface [14].

Using an iterative process, the precise size of the anchor and shear keys can be used to determine the weight needed to resist sliding, Q_{AD}, and the overturning moment, M_d (see Figure 5).
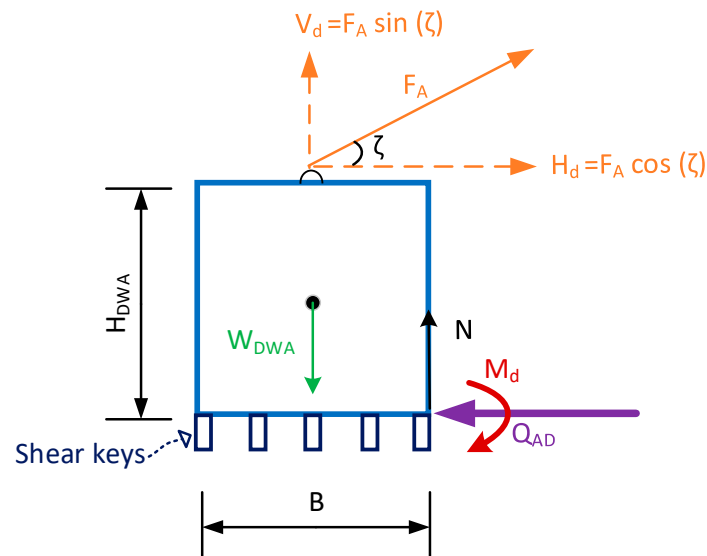

Figure 5. Free-body diagram of a deadweight anchor.

Preliminary Design

1. Initial parameters. The design criteria for DWAs are available in the literature as well as experimental design data [3,14,17]. In addition, the designer needs to gather the mechanical properties of the concrete, such as Young's modulus, E_c, and compressive strength, f'_c, among others. These parameters can be obtained from the concrete structure design codes and technical documents, for example, ACI 318-08 [41].

2. Structural analysis. A structural analysis of the system is carried out, based on the loads obtained. From this analysis, the mechanical elements of the system are obtained: axial force, shear force, overturning moment, and displacements.

3. Anchor weight. A preliminary anchor design is made. At this point, the Equations proposed by van Zwieten et al. [14] can be used. To resist sliding on cohesionless soils the required submerged weight, W_{DWA} is calculated using the following Equation:

$$W_{DWA} = \frac{H_d}{tan(\phi - 5°)} + V_d \tag{14}$$

where $H_d = F_A \cos(\zeta)$ is the horizontal component of the anchor loading, ϕ is the angle of internal friction of the sediment, and $V_d = F_A \sin(\zeta)$ is the vertical component of the anchor loading.

ζ is the angle between the anchor loading and a horizontal line.

4. Anchor diameter.

   Anchor without shear keys
   The minimum anchor width/diameter (B) can be determined by:

$$B = \left[\frac{6W_{DWA}H_d}{\gamma_c(W_{DWA} - V_d)} \right]^{\frac{1}{3}} \tag{15}$$

where γ_c is the submerged specific weight of the anchor material (concrete).

If shear keys in the DWA are required, see Appendix C. Maximum height: The maximum height, H_m, for the connection of the mooring line, above the base of the anchor, can be determined as suggested by Taylor [13] as:

$$H_m = \frac{B\,(W_{DWA} - V_d)}{6H_d} \tag{16}$$

The length of the cubical anchor needed to achieve the required weight can be determined by:

$$L_{DWA} = \frac{W_{DWA}}{\gamma_c\,H_m B} \tag{17}$$

The height of the cylindrical anchor needed to achieve the required weight can be determined by:

$$H_{DWA} = \frac{4W_{DWA}}{\gamma_c\,\pi\,B^2} \tag{18}$$

If the height H_{DWA} is greater than H_m, B should be modified; otherwise H_{DWA} is considered the height of the structure.

5. Overturning moment. The overturning moment of the structure, M_d, is determined based on following Equation:

$$M_d = W_{DWA}\left(\frac{B}{2}\right) - V_d\left(\frac{B}{2}\right) - H_d\,H_{DWA} \tag{19}$$

The load eccentricity , e, is determined using:

$$e = \frac{M_d}{V_d} \tag{20}$$

Geotechnical Capacity

In this part of the procedure proposed, the geotechnical capacity of the structure is determined, using the formulation indicated in DNV-OS-J101 [15].

6. Effective dimensions. To determine the bearing capacity, an effective base area is needed (see Appendix C). Bearing capacity: In fully drained conditions, the general formula below can be applied for the bearing capacity of a foundation with a horizontal base, resting on the soil surface:

$$Q_{\text{RAGD}} = \frac{1}{2}\gamma_{soil}b_{eff}N_\gamma s_\gamma i_\gamma + p_0'N_q s_q i_q + c_d N_c s_c i_c \tag{21}$$

where N_c, N_q, and N_γ are the bearing capacity factors, c_d design cohesion, i_γ, i_q, and i_c are the inclination factors, p_0' is the effective overburden pressure at the level of the foundation-soil interface, and s_γ, s_q, and s_c are shape factors (see Appendix C).

For undrained conditions, which imply $\phi = 0$, the following formula for the bearing capacity applies:

$$Q_{\text{RAGD}} = s_{ud}N_c^0 s_c^0 i_c^0 + p_0' \tag{22}$$

where N_c^0 is the bearing capacity factor, i_c^0 is the inclination factor, $p_0 = 0$ is the effective overburden pressure, s_c^0 is the shape factor, and s_{ud} is the undrained strength of the design, assessed from the actual shear strength profile, load configuration, and estimated depth of the surface that potentially fails (see Appendix C).

7. Sliding capacity. The sliding capacity for drained conditions can be determined by the following Equation:

$$Q_{RLGD} = \left(c_d A_{eff} + V_d \tan(\phi)\right)\mu \tag{23}$$

In the case of undrained soils:

$$Q_{RLGD} = \mu\left(s_{ud}A_{eff}\right) \tag{24}$$

More detailed research on how to determine the sliding capacity for this type of structure can be found in [42,43].

8. Design revision. The acting forces (V_d, H_d) must be less than the resistant axial and sliding forces (Q_{RAGD}, Q_{RLGD}). If this condition is not fulfilled, the preliminary design is modified, and the design process started again.

Structural Capacity

9. Axial capacity (structural). The tensile capacity, Q_{RASD}, of the structure is determined using the following Equation ACI 318-08 [41]:

$$Q_{RASD} = 0.8\left(\vartheta \sqrt{f_c'}\right) A_P \tag{25}$$

where A_p is the cross-sectional area of the anchor (DWA) and ϑ is a parameter defined based on the type of concrete (ACI 318-08 [41]).

10. Lateral capacity (structural). The shear-resistant capacity, Q_{RLSD}, of the anchor is determined using the following Equation [41]:

$$Q_{RLSD} = \phi_{vc}\left[0.17\left(1 + \frac{V_d}{3.5\,A_p}\right)\xi\sqrt{f_c'}Bd\right] \tag{26}$$

with the characteristic length ($d = 0.8$). Where ϕ_{vc} is the resistance factor for shear design (typically 0.75), and ξ is a modification factor reflecting the reduced mechanical properties of concrete [41].

11. Sliding capacity. The sliding capacity can be determined by (see Figure 5):

$$Q_{RSSD} = \mu\,N_f = \mu\left[W_{DWA} - V_d\right] \tag{27}$$

where N_f is the normal force, and μ is the friction coefficient.

Revision of structural capacity. The resistant axial (Q_{RASD}) and lateral capacity (Q_{RLSD}) must not be exceeded by the design load, (V_d, H_d) If these conditions are not fulfilled, the geometry of the structure must be changed, and the design process must be started again. In addition, the capacity should be checked for sliding ($Q_{RSSD} \geq H_d$).

2.2. Service Limit State Design

The following is to determine whether the anchor satisfies the displacements and rotations for the service limit state (SLS) of the case of piles.

2.2.1. Pile Anchors
P–Y Curves

In order to satisfy the SLS conditions, the long-term behavior of the piles must be analyzed, based on DNV-OS-J101 [15]. The main parameters are the accumulated rotation, ς_{acc}, and deflection, y_{acc}, or, equivalently, the strain accumulation at the mudline level. To determine the deflections of the piles, p–y curves are generally used [44–46]; this methodology is based on the Winkler approach [47]. These curves are commonly defined for clayey and sandy soils, but in the case of weak rocks, such as weak mudstone, sandstone, and carbonate materials, different formulations for P–Y curves have been proposed (see Table 1). Appendix B shows the procedure to determine the P–Y curve for the case of weak rock.

Table 1. Reference for P–Y curve construction for various rocky soils.

Type of Soil	Reference for P–Y Curves
Calcareous	Wesselink et al. [48]
	Williams et al. [49]
	Dyson and Randolph [50]
Weak rock	Reese [25]
Weak carbonate rock	Abbs [27]
Weak calcareous claystone	Fragio et al. [51]
Strong rock	Turner [52]
Massive rock	Liang et al. [53]

As the contribution of the shaft resistance and base resistance are not considered in this procedure [3,17], p–y curves do not apply for large-diameter piles. These curves predict the stiffness of the structure [45], which can have a direct impact on the calculated deformations, rotations and dynamic properties of the pile. For this reason, many researchers have been developing design procedures for large-diameter stock piles, for instance, Zdravković et al. [54] and Byrne et al. [55]. Procedures to calculate deflections and rotations on weak rock have been provided by various authors; for instance, Ashour et al. [56] and Carter and Kulhawy [28] studied the behavior of flexible and rigid shafts socketed into rock, subject to lateral loads and overturning moments. Zhang et al. [30] extended this approach to predict the nonlinear lateral load-displacement response of rock socketed shafts. The procedure considers subsurface profiles consisting of a soil layer overlying rock.

After calculating long-term deflections and rotations, these are compared to the maximum loads allowed in the design codes. The initial deflection, y_o, and accumulated deflection, y_{acc}, must be less than 0.2 m; the initial rotation, ς_0, must be less than 0.5°, and the accumulated rotation, ς_{acc}, must be less than 0.25° [3,17]. If these criteria are not met, the pile geometry must be modified, and the design process restarted.

2.2.2. Deadweight Anchors

One of the most significant parameters in determining whether the DWA satisfies the SLS is the formation of cracks. DNV-OS-C502 [35] states that design parameters do not cause permissible damage to the anchor due deflections and vibrations. This guarantees that the behavior allows the ocean current turbine to generate the amount of electrical energy it was designed to produce. To check that any cracks in the concrete structure are not significant, DNV-OS-C502 [35] proposes the following condition:

$$\sigma_1 \leq \frac{f_{tn}}{k_1} \tag{28}$$

where σ_1 is the principal tensile stress, f_{tn} is the normalized structural tensile strength of concrete, and k_1 is a constant value used in the calculations of crack (Table O3) DNV-OS-C502 [35].

In the event of the combined action of axial stress and bending moment, the following condition must be satisfied:

$$(k_w\sigma_N + \sigma_M) < k_w \frac{f_{tn}}{k_1} \tag{29}$$

where σ_N is the stress due to axial force (positive tension), σ_M is the edge stress due to bending alone (positive tension), and k_w is the coefficient dependent on cross-sectional height, defined by:

$$k_w = 1.5 - \frac{h}{h_1} \geq 1.0 \tag{30}$$

where $h_1 = 1.0$ m.

2.3. Fatigue Limit State Design

2.3.1. Fatigue Analyses

Fatigue analyses are used to estimate the number of loadings cycles the structure can withstand during its lifetime. This is usually carried out using either the accumulated damage model (i.e., Miner's rule) or a detailed fracture mechanical study. In cases where the maximum stress amplitude does not exceed the fatigue limit amplitude for 107 cycles DNV-RP-C203 [34], or in early design stages, the accumulated damage model based on S–N curves might be sufficient.

In this study, the accumulated damage model is used, which is based on S–N curves. More detail can be found in DNV-OS-J101 [15]. As wave forces are the main cause of fatigue damage in offshore structures, other factors, such as periodic changes of wind and currents, are often neglected. In cases where the influence of other environmental factors should not be ignored, a more advanced fatigue model, based on simulations, might be the better choice, as per DNV-OS-J101 [15]. The accumulated damage model separates the sea states into different blocks of the same wave height and period, with their corresponding return period, T_R. In industry, often only the wave height is used to define the block. In such cases, the corresponding wave period should be estimated accordingly. Miner's rule gives the accumulated damage D_R in the reference period by:

$$D_R = \sum_{i=1}^{I} \frac{n_i}{N_i} \tag{31}$$

where n_i denotes the number of load cycles in the i-th block, i is the total number of blocks.

The design life N_i can be understood as the number of load cycles which would damage the structure with the same loads as in the i-th block. The number of load cycles (n_i) can be estimated by:

$$n_i = T_R \frac{p_i}{T_i} \tag{32}$$

where p_i is the relative probability of the i-th block and T_i is the wave period corresponding to i-th block. In this study, the simplified block definition, based only on wave height, is used. Therefore, the corresponding wave period must be estimated. DNV-OS-J101 [15] gives a possible range of periods for a given significant wave height. To obtain conservative results, the lower boundary for the wave period is chosen:

$$T_i = 11.1 \sqrt{\frac{H_i}{g}} \tag{33}$$

where H_i denotes the wave height of the i-th block and g the gravitational acceleration.

The period corresponding to the service life, T_L, of the structure can then be obtained by:

$$T_L = \frac{T_R}{D_R} \tag{34}$$

2.3.2. S–N Curves

Steel Anchors

Steel anchors generally consist of a steel tube with a pad-eye welded to the top end of the tube. The holes, joints, and especially the welds are prone to crack under load conditions and should be analyzed accordingly. S–N curves for welded joints are defined in DNV-RP-C203 [34] and DNV GL-ST-0126 [57]. The design life, N_i (predicted number of load cycles to failure), of the weld is defined by:

$$\log N_i = \log \bar{a} - m \log \left(\Delta \sigma_{i,f} \left(\frac{t}{t_{ref}} \right)^k \right) \tag{35}$$

with the cyclic load range, $\Delta\sigma_{i,f}$, given by:

$$\Delta\sigma_{i,f} = \sigma_{i,max} - \sigma_{i,min} \tag{36}$$

where t is the material thickness, t_{ref} the reference thickness, $\sigma_{i,max}$ and $\sigma_{i,min}$ the maximum and minimum stresses in the weld due to cyclic loads, respectively.

The factors k, $\log\bar{a}$, and m depend on the number of load cycles and the type of welding and can be taken from Table 2-2 and Table 2-3 in DNV-RP-C203 [34] (page 14f). For welds parallel to the stress direction, S–N curves of C1 type should be used. For welds perpendicular to the stress direction and flush-ground welds, S–N curves of C1 type are also used, while curves D and E should be used for perpendicular welds not greater than 10% and 20% of the weld′s width, respectively.

Concrete Anchors

S–N curves for the design life of offshore concrete structures (reinforced and unreinforced) can be found in DNV-OS-C502 [35]. If made of concrete, DWAs are normally not reinforced, for which the corresponding S–N curves are defined as:

$$log_{10}N_i = C_1 \frac{1 - \frac{\sigma_{i,max}}{f_{rd}}}{1 - \frac{\sigma_{i,min}}{f_{rd}}} \tag{37}$$

where N_i is the predicted number of load cycles to failure, f_{rd} is the compressive strength for the specific failure type, $\sigma_{i,max}$ the maximum compressive stress, and $\sigma_{i,min}$ the minimum compressive stress.

The minimum compressive stress should be considered as zero in case of tension (i.e., negative values). C_1 should be taken as 10 when $\sigma_{i,max}$ and $\sigma_{i,min}$ are both positive (i.e., compression-compression load case) and as 8 when σ_{min} is negative (i.e., compression-tension load case). In case $\log N_i$ is greater than χ, which is defined as:

$$\chi = \frac{C_1}{1 - \frac{\sigma_{i,min}}{f_{rd}} + 0.1C_1} \tag{38}$$

The design life can be extended to:

$$logN_i' = C_2 logN_i \tag{39}$$

where N_i' is the extended design life and the factor C_2 is given by:

$$C_2 = \left(1 + 0.5\left(\log_{10}N_i - \chi\right)\right) \geq 1.0 \tag{40}$$

3. Application of the Design Procedure

This section details the design procedure as applied to pile and DWA-type anchors for an ocean current turbine. The PA cross-section is circular, hollow, and made of steel, while the DWA is cylindrical in shape and made of concrete.

3.1. Case Study

In Mexico, the most suitable site for the deployment of ocean current turbines is off Cozumel Island, in the Caribbean Sea [9], as there is a persistent current from the NE. Data on the water depth in the shallow regions of the Cozumel Channel close to Cozumel Island can be found in [10,12]. In April 2019, a bathymetric survey was carried out as part of the CEMIE-O 1 research expedition around Cozumel Island. The multibeam echo sounder, Kongsberg ES 302, was used to gather the data presented in Figure 6. Across the transection, marked P1 on the mainland side and P2 on the island side, a bathymetric profile of the Cozumel Channel is given (see Figure 7). The raw data were interpolated using the function *griddata* and its cubic interpolation method, which is part of the *scipy.*

interpolate Python module [58]. In the first phase of the project, a small-scale turbine is to be installed in the shallower region, close to P2, as suggested in [10]. At those depths, the seabed is composed of a thin layer of fine sand with limestone below [12]. In the second phase of the project, a full-size turbine will be installed in the central part of the channel at water depths of about 400 m, for which a fixed structure is unfeasible, so a floating design is needed for the small-scale turbine as well; the marine current data were obtained from [10]. The turbine used in this example is an ocean current.
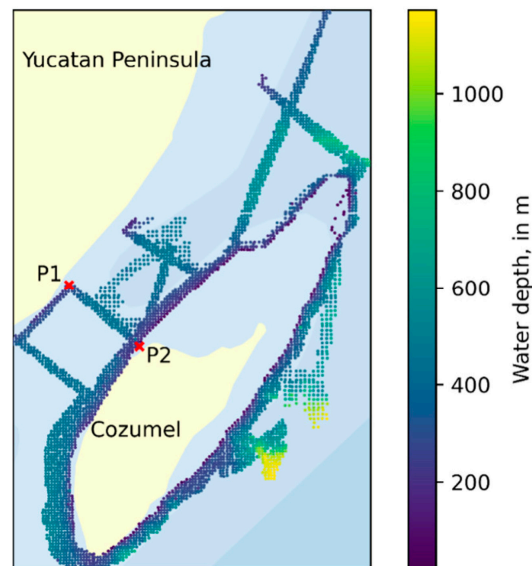
Figure 6. Bathymetric Survey carried out in the CEMIE-O 1 research expedition, April 2019. Background data from Natural Earth.
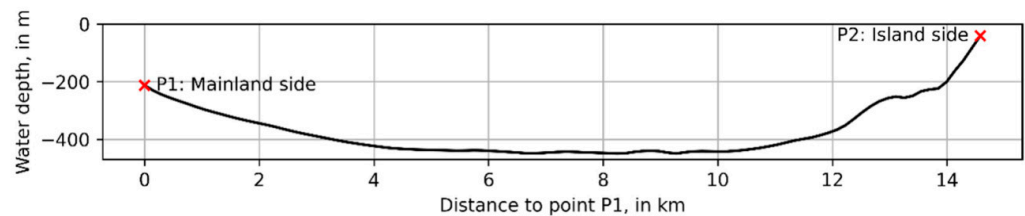
Figure 7. Bathymetric cross section of the Cozumel Channel. 5 times vertically enlarged.

The main difference between the ocean current turbine used in this example and other ocean current turbines is the persistence of the harnessed current. Generally, this type of turbine must adapt to a shift in the direction of the current every six or 12 h, depending on the location. The turbine discussed, off Cozumel, is not subject to significant shifts in the current. The turbine is installed on a platform of two floaters that provide the necessary buoyancy, and a strut connecting them with the turbine. The platform is moored to the seabed by cables and anchors, with the axis of the turbine aligned parallel to the flow. The turbine has three blades, and its rotor has a diameter of $d_r = 1$ m; in addition, this device will be anchored at a water depth of h = 35 m, 20 m above the seabed [10]. It is considered that the maximum deflection of the turbine from its equilibrium position (i.e., without environmental loads such as waves and currents) will not exceed 0.5 m in the vertical. The platform is attached to four mooring lines which, lower down, join into a single line which is attached to the anchor. In this way, the anchor only needs to resist the forces on the single line.

Table 2 summarizes the mechanical properties of the materials used, the soil found on the construction site, and the principal data of the turbine.

Table 2. Design parameters.

Parameter	Symbol	Value	Unit
Structural Steel (A36)			
Yield stress	F_y	25	MPa
Tensile strength	F_u	400	MPa
Modulus of elasticity of steel	E_s	200	GPa
Specific weight	γ_s	7860	kN m^{-3}
Structural concrete			
Concrete Compressive Strength	f_c'	35	MPa
Specific weight	γ_c	23.6	kN m^{-3}
Limestone			
Specific weight	γ_s'	26.5	kN m^{-3}
Coefficient of subgrade reaction	n_h	80	MN m^{-3}
Sand			
Internal friction angle of the soil	ϕ	30	degrees
Specific weight	γ_s'	17	kN m^{-3}
Effective overburden pressure	p_0'	10	kN m^{-2}
Material factor	γ_ϕ	1.2	-
Friction coefficient	μ	0.5	-
Turbine			
Rotor diameter	d_r	1	m
Drag coefficient	C_D	8/9	-
Length of mooring line	l_M	20	m
Allowed vertical deflection	d_v	0.5	m
Design depth of operation	z	10	m
Environment			
Design ocean current	v_c	2.5	m s^{-1}
Design tidal current	v_t	0	m s^{-1}
Design wave height	DWH_d	7	m
Design wave period	T_d	9	s
Design wind speed at 10 m height	v_{10m}	15	m s^{-1}
Local water depth	d	30	m
Water density	ρ_w	1025	kg m^{-3}

3.2. Design Considerations

The design requirements for anchors of ocean current turbines depend on many different factors. Their description and evaluation are beyond the scope of this work. Detailed information on design values or the required return period of the sources of environmental loads, and their respective load factors can be found in technical documents and design codes, such as IEC 62600-2 [59]. In the following section, the environmental loads are highly simplified, the purpose being solely to generate a representative load case and demonstrate the behavior of the design procedure presented. Eventually, these simplified approaches should be replaced by a more comprehensive mooring study for real problems, but they do give valuable insight into expected loads for the early stages of the design process. For those studies, mooring simulation tools can be used, such as ProteusDS [60]. Furthermore, the design is based only on a single load case, where the turbine is operating at its design depth and subject to the effects of the design current, design wave, and design wind. All load cases can be found in [59].

3.2.1. Environmental Interaction

Ocean current turbines and their anchors are subject to loads from a wide range of sources, such as hydrostatic pressure, currents, waves, tides, wind, ice, earthquakes, and collision with man-made objects. The considered construction site is not a seismic area, thus loads due to seismic actions can be ignored. Furthermore, this work only considers

environmental loads that are transmitted by the mooring line to the anchor; however, in some cases, direct interaction of the anchor with the water may be necessary to consider. For subsurface moorings, the environmental loads are caused primarily by the local velocity of the water. Hence, regarding environmental loads, this work is focused on water velocity and its main drivers: ocean currents, tidal currents, waves, and wind. Ocean currents are part of the oceanwide circulation systems and are caused by prevailing winds, and gradients in temperature and salinity. Tidal currents are a result of the periodic rise and fall of the water level and depend highly on the bathymetry and geometry of the ocean basin [61]. Based on IEC 62600-2 [59], the velocity at hub height can be understood as the vector sum of those four sources:

$$\vec{v}_\infty = \vec{v}_c + \vec{v}_t + \vec{v}_w + \vec{v}_a \tag{41}$$

where $\vec{v}_\infty$ denotes the undisturbed velocity, $\left(\vec{v}_c\right)$ is the velocity of the ocean current, $\left(\vec{v}_t\right)$ is the tidal velocity, $\vec{v}_w$ is the wave induced velocity, and $\vec{v}_a$ is the wind induced velocity.

The velocity of the ocean current and the tidal velocity can be taken from technical documents or can result from extreme value analysis. Both the induced velocity from waves and from wind can be indirectly estimated via parameters of the design wave and design wind, as shown below. It should be mentioned that additional to those four drivers, the engineering design may need to evaluate other drivers or even non-linear velocity components as well.

3.2.2. Wave-Induced Velocity

Both Airy wave theory and the second-order wave theory give precise results for the requirements of most offshore engineering problems [17]. Waves induce velocities in horizontal (i.e., in direction of wave propagation) and vertical directions, both of which are periodic in nature. Applying the second-order wave theory, maximum and minimum horizontal velocities are defined as:

$$v_w = \pm\zeta_a\omega\frac{\cosh(\kappa(d-z))}{\sinh(\kappa d)} + \frac{3}{4}\zeta_a^2\kappa\omega\frac{\cosh(2\kappa(d-z))}{\sinh^4(\kappa d)} \tag{42}$$

where ζ_a denotes the wave amplitude, ω is the angular frequency, κ the wave number, d the local water depth, and z the depth below the mean sea level (MSL).

The linear term in Equation (42) is taken as positive for the maximum velocity, and negative for the minimum velocity.

3.2.3. Wind-Induced Velocity

Based on IEC 62600-2 [59], wind effect is negligible in 20 m depth and below. The induced velocity is a result of wind shear [61] and presents a linear behavior in the upper 20 m of the water column [15]:

$$v_a = 0.01 v_{a,ref}\left(1 - \frac{z}{20}\right) \tag{43}$$

where $v_{a,ref}$ is the one hour mean wind speed 10 m above MSL and z the depth below MSL.

3.2.4. Horizontal Force on the Mooring System

To extract energy from the current flow, its momentum must be changed, requiring a drag force to be exerted on the flow. The related reactional force, exerted by the current on the rotor, has an axial and radial component with respect to the rotational axis of the rotor. The radial component creates the torque, which is used to generate electricity, while the axial component can be understood as rotor drag. Considering only the case where the turbine is in operational mode, the drag force can be conservatively estimated following Betz Law [62]. Assuming the rotor is operating at the maximum theoretical

power coefficient, $C_P = 0.59$, the rotor drag coefficient can be estimated as $C_{drag} = \frac{8}{9}$ [63]. Thus, the drag force is:

$$F_D = \frac{4}{9}\rho_w v_\infty^2 A_r \tag{44}$$

where A_r is the sweep area of the rotor, and ρ_w is the density of water.

For ocean current turbines, the rotor thrust accounts for roughly 81% of the total horizontal load of the system [14]. Hence, the thrust force, F_H, can be estimated using the following Equation:

$$F_H = \frac{F_D}{0.8} = \frac{5}{9}\rho_w v_\infty^2 A_r \tag{45}$$

3.2.5. Total Force on the Mooring System

The loads affecting the mooring system require detailed analysis and simulation, which is usually performed with specialized tools, such as ProteusDS software [60]. However, this study concentrates on the design of the anchor and the estimation of the loads on the anchor using simple physical relations and assuming a single mooring leg design. The total force on the mooring line is a function of the horizontal force estimated with Equation (45) and of the vertical load due to the buoyancy of the platform.

The mooring line is idealized as a straight line and ignoring the submerged weight of the mooring line and fluid loading for simplicity, the load on the mooring line is equal to the load on the anchor. In Figure 8a, the deflection of the system due to the horizontal load is depicted. Figure 8b shows the free body diagram of the turbine and the anchor point, assuming no elongation of the mooring line. Based on this and simple geometric relations, the required buoyancy force needed to limit the vertical deflection to d_v under the horizontal load, F_H, can be calculated as:

$$F_B = \frac{F_H(l_M - d_v)}{\sqrt{2l_M d_v - d_v^2}} \tag{46}$$

The resulting force on the mooring line (F_M) can then be derived from:

$$F_M = F_B\frac{l_M}{l_M - d_v} \tag{47}$$

Under the given assumptions, the total force, F_A, must be equal to the force on the mooring line, F_M:

$$F_A = \gamma\frac{F_H\, l_M}{\sqrt{2l_M d_v - d_v^2}} \tag{48}$$

where l_M denotes the length of the mooring i.e., the height above seabed in its initial position, d_v is the maximum vertical displacement allowed, towards the platform, γ is the resistance factor, and F_H is the horizontal force.

The effective angle of the mooring, α_M, from the vertical can be determined by:

$$\alpha_M = \arccos\left[1 - \frac{d_v}{l_M}\right] \tag{49}$$
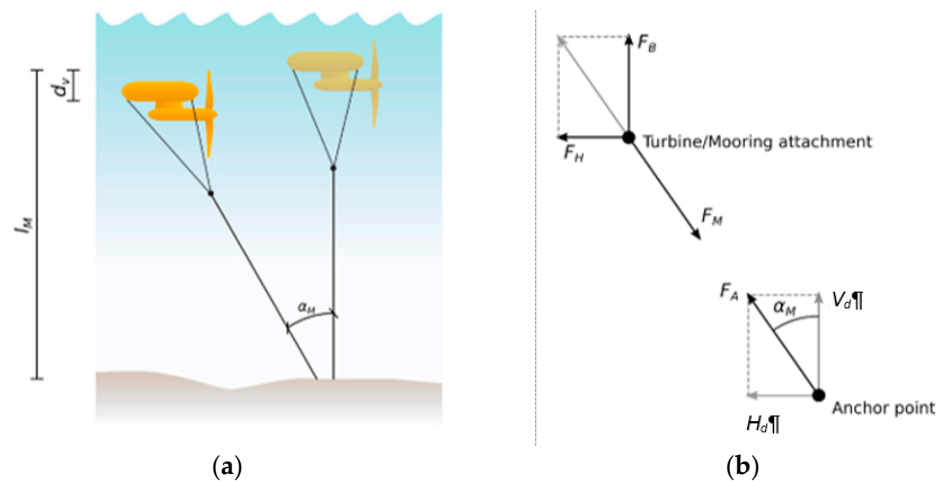
Figure 8. (**a**) Deflection of mooring system under horizontal load. (**b**) Free body diagram of turbine/mooring attachment point and anchor point.

3.3. Design Results and Discussion

A summary of the design results is presented in Table 3. To perform the calculations, SMath [64] was used.

As can be seen in the design procedure, it is the structural component which determines the design in pile, because the structural strength is higher compared to the geotechnical capacity. In the case of the DWA, the opposite behavior is presented; this is because this anchor is not directly in contact on limestone, but there is a sand layer. The Figure 9 shows the P–Y curve, where, for a horizontal load of 43 kN (load design), the approximate deflection is 1 mm, so the pile behavior is linear elastic. Therefore, the maximum allowable deflection of 20 cm is satisfied.

Figure 10 gives a comparison between diameter and weight as a function of the strength of the structure. As can be seen, steel piles have greater strength than DWAs of the same diameter. However, the weight of the structure is significantly more, which can have a direct effect on the cost of construction and transportation.

Table 3. Design results.

Parameter	Symbol	Value	Unit	Equation
Load Design				
Final load of system	F_A	100.0	kN	(48)
Pile				
Diameter	D_P	10.0	cm	-
Wall thickness	t_P	7.6	mm	(1)
Area moment of inertia	I_P	243.0	cm^4	(A1)
Embedded length	L_r	144	cm	(2)
Surface area of the pile shaft	A_f	4606	cm^2	
Weight	W_P	184.0	kN	
Axial capacity (structural)	Q_{RASP}	428.1	kN	(3)
Lateral capacity (structural)	Q_{RLSP}	128.4	kN	(4)
Axial capacity (geotechnical)	Q_{RAGP}	4120.7	kN	(13)
Lateral capacity (geotechnical)	Q_{RLGP}	454.6	kN	

Table 3. *Cont.*

| Parameter	Symbol	Value	Unit	Equation
Dead Weight Anchor				
Weight	W_{DWA}	188.2	kN	(14)
Diameter	B	2.00	m	(15)
Height of the mooring line connection point	H_m	1.92	m	(16)
Height of the cylindrical anchor	H_{DWA}	2.03	m	(18)
Overturning moment	M_d	58.9	kN-m	(19)
Axial capacity (geotechnical)	Q_{RAGD}	231.2	kN	(21)
Sliding capacity (geotechnical)	Q_{RLGD}	26.5	kN	(23)
Axial capacity (structural)	Q_{RASD}	10190	kN	(25)
Lateral capacity (structural)	Q_{RLSD}	2113.7	kN	(26)
Sliding capacity (structural)	Q_{RSSD}	22.4	kN	(27)
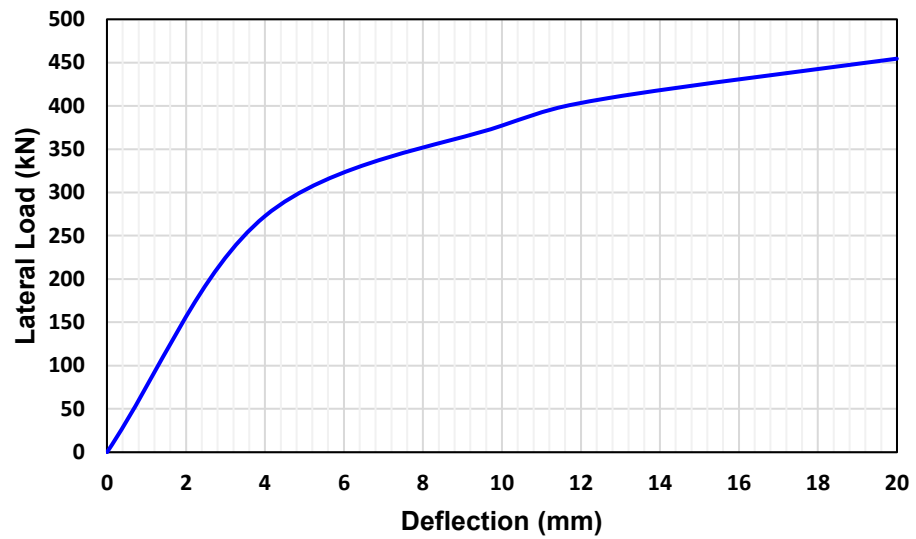
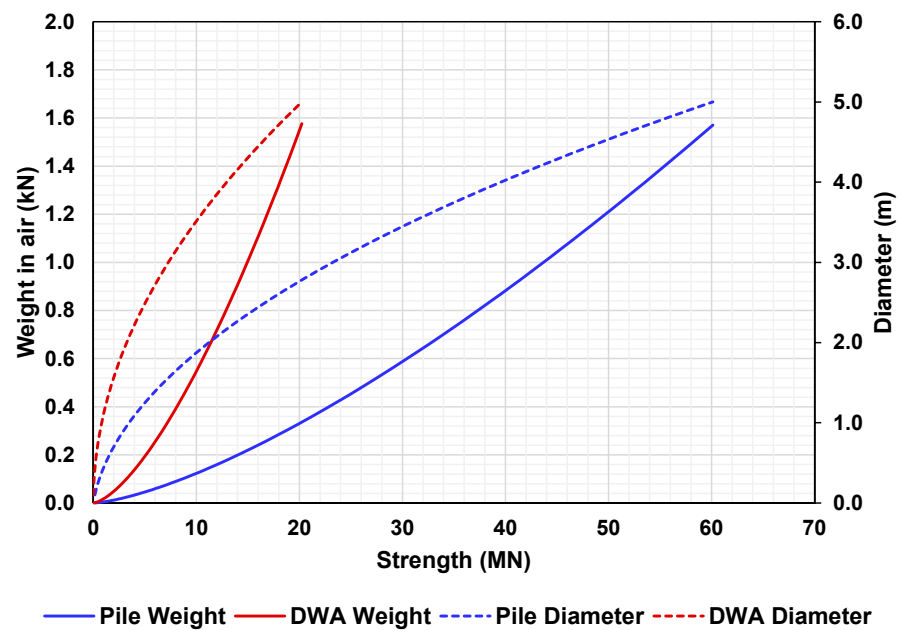**Figure 9.** P–Y curve of pile application example.

Figure 10. Comparative graph of the resistance and diameter of the anchors.

4. Conclusions and Recommendations

A new design procedure for ocean current turbines anchors on weak rock was proposed. It is easy to apply, since it uses Equations provided in technical documents and design codes that are normally used in industry; it is also possible to use tools common in the design of structures, such as spreadsheets. The iterative procedure consists of a preliminary anchor design that can be modified to satisfy the limit states considered. From the preliminary geometry, the structural capacity is determined, followed by the geotechnical capacity on rock to resist the loads corresponding to ULS. Finally, the anchor is revised against the requirements for the SLS and FLS.

The proposed procedure was applied for a turbine prototype to be deployed off Cozumel Island, Mexico. A floating turbine with a single mooring line was chosen for this project, as this enables the device to be passively oriented in the marine current. Great differences between the anchors were seen in terms of their weight and dimensions. The lack of slope at the installation site makes the use of a DWA feasible. The required weight for a DWA is significantly higher than that of the pile anchor, and this is directly proportional to the cost of the anchor, making this a relevant consideration. Although the cost of the material is an important parameter for the choice of anchor, there are other parameters to consider, such as availability of raw materials, manufacturing costs, transportation, installation, and decommissioning (if required). The following conclusions can be drawn:

(e)   Both anchor designs showed satisfactory results based on the stipulations in the relevant design codes and technical documents. However, to guarantee this conclusion, it is necessary to carry out additional design tests.

(f)   For relatively small projects, DWAs are the better option. In larger projects, piles are more suitable, especially if the dimensions of the DWA mean that expensive transportation and installation equipment are required.

(g)   The deflection presented in the pile satisfies the maximum permissible value corresponding to the recommendations indicated in the technical documents for marine structures design.

Author Contributions: Conceptualization and methodology, F.B.-G. and M.R.; model and validation, F.B.-G. and M.R.; writing—original draft preparation, F.B.-G. and M.R.; writing—review, E.M. and R.S. All authors have read and agreed to the published version of the manuscript.

Conflicts of Interest: The authors declare no conflict of interest.

Nomenclature

Symbol	Description
$\vec{v}_\infty$	undisturbed current speed
$\vec{v}_a$	wind induced velocity
$\vec{v}_c$	current velocity
$\vec{v}_t$	tidal velocity
$\vec{v}_w$	wave induced velocity
h_1	parameter defined as 1.0 m
A_{eff}	effective area
A_f	surface area of the pile shaft
A_p	cross-sectional area of anchor
A_r	area of rotor sweep

Symbol	Description
C_1	type of cyclic stress factor
C_2	extended lifetime factor
C_{drag}	drag coefficient of the rotor
C_p	power coefficient
D_P	pile diameter
D_R	accumulated damage
DWH_d	design wave height
E_c	Young′s modulus of concrete
E_{ir}	Initial modulus of rock
E_s	Young′s modulus of steel
F_A	final load on the anchor
F_B	required buoyancy force
F_D	maximum theoretical drag
F_H	load produced by the turbine chain
F_M	resulting force on the mooring line
F_{cr}	critical strength
F_u	ultimate stress
F_y	yield stress
H_{DWA}	height of the cylindrical anchor
H_d	horizontal anchor loading
H_i	wave height of the *i*-th block
H_m	maximum height of the mooring line connection point above the base of the anchor
I_P	area moment of inertia of the pile cross section
K_p	passive earth pressure coefficient
L_{DWA}	length of the cubical anchor
L_r	embedment length
M_d	overturning moment
N_c, N_γ, N_q	bearing resistance factor for drained conditions
N_c^0	bearing resistance factor for undrained conditions
N_f	normal force
N_i	number of load cycles which would damage the structure under same load patterns as in the *i*-th block
N_i'	number of load cycles which would damage the structure under same load patterns as in the *i*-th block, considering extended design life
Q_{RAGD}	axial structural capacity of DWA
N_i	number of load cycles which would damage the structure under same load patterns as in the *i*-th block
N_i'	number of load cycles which would damage the structure under same load patterns as in the *i*-th block, considering extended design life
Q_{RAGD}	axial structural capacity of DWA
Q_{RAGP}	axial geotechnical capacity of pile
Q_{RASD}	axial structural capacity of DWA
Q_{RASP}	Axial structural capacity of pile
Q_{RLGD}	sliding geotechnical capacity of DWA
Q_{RLGP}	lateral geotechnical capacity of pile
Q_{RLSD}	lateral geotechnical capacity of DWA
Q_{RLSP}	Lateral structural capacity of pile
Q_{RSSD}	sliding structural capacity of DWA
Q_f	ultimate shaft resistance
T_L	period of service life
T_R	reference period
T_d	design wave period
T_i	wave period corresponding to *i*-th block
V_d	vertical anchor loading
V_d'	lateral capacity of a deadweight anchor with full-base keying skirts in cohesionless soil

Symbol	Description
W_{DWA}	submerged weight of dead weight anchor
W_k	submerged weight of each shear key
W_p	submerged weight of pile
Z_s	depth to the bottom of the skirts
$\bar{a}$	Factor, directly related to intercept of log N-axis of S–N curve ($\log \bar{a}$)
b_{eff}, l_{eff}	effective dimensions
c_d	design cohesion
d_v	maximum permitted vertical deflection of the platform
f_c'	compressive strength of concrete
f_l	limiting skin friction
f_{rd}	compressive strength of concrete for specific failure type in fatigue analysis
$f_{s,limit}$	peak post-cyclic shear strength
f_{tn}	normalized structural tensile strength of concrete (Table C1) DNV-OS-C502
i_c^0	inclination factor for undrained conditions
i_γ, i_q, i_c	inclination factors for drained conditions
k_1	constant, used in calculations of crack width (Table O3) DNV-OS-C502
k_{ir}	dimensionless coefficient defined by Equation (A5)
k_{rm}	dimensionless coefficient in the range of 0.0005 and 0.00005
k_w	coefficient dependent on cross-sectional height
l_M	length of the mooring
l_e, b_e	dimensions defined in Appendix C
l_{eff}, b_{eff}	effective dimensions in Appendix C
n_h	horizontal coefficient of subgrade reaction of the soil
n_i	denotes the number of load cycles in the *i*-th block
n_{sk}	number of shear keys
p_0'	effective overburden pressure at the level of the foundation-soil interface
p_a	elastic lateral pile resistance
p_i	relative probability of the i-block in fatigue analysis
p_u	ultimate pile resistance
q_e	embedment force of shear keys
q_u	soil's uniaxial unconfined strength
s_c, s_q, s_γ	shape factors for drained conditions
s_c^0	shape factor for undrained conditions
s_u	undrained shear strength
s_{ud}	design undrained strength assessed based on the shear strength profile
t_P	pile wall thickness
t_k	shear key thickness
t_{ref}	reference thickness
v_{10m}	design wind speed at 10 m height
v_a	induced velocity
$v_{a,ref}$	one hour mean wind speed 10 m above MSL
v_c	design ocean current
v_t	design tidal current
v_w	maximum and minimum horizontal velocity
y_a	elastic limit pile deflection
y_{acc}	accumulated pile deflection
y_o	initial pile deflection
y_u	ultimate pile deflection
α_M	effective angle of the mooring
α_r	strength reduction factor
γ_c	submerged specific weight of the anchor material (concrete)
γ_k	specific weight of the anchor shear keys
γ_s	specific weight of structural steel
γ_{soil}	submerged unit weight of soil

Symbol	Description
γ_w	specific weight of water
ζ_a	wave amplitude
ρ_w	water density
ς_0	initial pile rotation
ς_{acc}	pile's accumulated deflection rotation
σ_1	principal tensile stress
σ_M	edge stress due to bending alone (positive tension)
σ_N	stress due to axial force (positive tension)
$\sigma_{i,max}$	maximum stress due to cyclic load for i-th block in fatigue analysis
$\sigma_{i,min}$	minimum stress due to cyclic load for i-th block in fatigue analysis
ϕ_d	parameter defined by Equation (A26)
ϕ_s	tangent of the friction angle at depth Z_s.
$\phi_{t,\,y}$	resistance factor for axial tensile strength (0.95)
ϕ_{vc}	resistance factor for shear strength for concrete anchor (0.75)
ϕ_{vs}	resistance factor for shear strength for steel anchor (0.9)
h	cross-section height
w	friction angle between the soil and the pile wall
B	minimum anchor width/diameter
K	coefficient of lateral earth pressure
N	number of layers
RQD	rock quality designation
c	cohesion of the soil
d	local water depth
e	eccentricity of the vertical force
f	unit outside shaft friction
g	gravitational acceleration
i	total number of blocks
k	exponent on thickness, for fatigue analysis
m	negative inverse slope of S–N curve
p	load per pile length unit
t	material thickness
y	pile deflection
z	depth below MSL
$\Delta\sigma_{i,f}$	cyclic load range for i-th block in fatigue analysis
α	adhesion factor
δ	steel-chalk interface friction coefficient
ζ	angle formed between the turbine chain and the anchor
κ	wave number
μ	friction coefficient
$\tilde{\varsigma}$	modification factor that reflecting the reduced mechanical properties of concrete, ACI 318-08
ς	pile rotation
χ	dimensionless parameter
ω	angular frequency
ϑ	parameter defined based onthe type of concrete
ϕ	internal friction angle of the sediment
$\phi\prime$	post peak internal soil friction coefficient

Appendix A

This Appendix shows some complementary Equations to calculate the geometrical and mechanical properties of piles anchors.

Second moment of area. The area moment of inertia of the pile cross section, I_p, can be determined using the following expression:

$$I_P = \frac{1}{8}\left(D_p - t_p\right)^3 t_p \tag{A1}$$

The surface area of the pile shaft, A_f, can be obtained using the following Equation:

$$A_f = \pi L_r D_p \tag{A2}$$

Pile weight. The submerged weight of the pile (W_p) is determined by:

$$W_p = A_p L_r (\gamma_s - \gamma_w) \tag{A3}$$

where γ_s is the specific weight of steel and γ_w is the specific weight of seawater.

Appendix B

In the case of weak rock, the shape of the p–y curve is based on Reese [25] and is made up of three sections of behavior (see Figure A1). The first section corresponds to the elastic range, the second to non-linear behavior, and the third to when pile stiffness is lost. The input parameters that define the curve are given in Table A1.

Table A1. Parameters that define p–y curves on weak rock.

Parameter	Symbol	Unit
Uniaxial unconfined strength	q_u	kPa
Strength reduction factor	α_r	-
Dimensionless coefficient in the range of 5×10^{-4} and 5×10^{-5}	k_{rm}	-
Initial modulus of the intact rock	E_{ir}	kPa

The elastic section of the curve, with deflections $y \leq y_a$ is given by:

$$p = k_{ir} E_{ir} y \tag{A4}$$

where k_{ir} is a dimensionless coefficient that accounts for changes, given by:

$$k_{ir} = \begin{cases} 100 + 400 \frac{z}{3D_p} & 0 \leq z \leq 3D_p \\ 500 & z > 3D_p \end{cases} \tag{A5}$$

The elastic limit displacement, y_a, is given by:

$$y_a = \left(\frac{p_u}{2 \, k_{ir} \left(k_{rm} D_p \right)^{0.25}} \right)^{4/3} \tag{A6}$$

where p_u is the ultimate lateral resistance, taken as:

$$p_u = \begin{cases} \alpha_r q_u D_p \left(1.0 + 1.4 \frac{z}{D_p} \right) & 0 \leq z \leq 3D_p \\ 5.2 \alpha_r q_u D_p & z > 3D_p \end{cases} \tag{A7}$$

The parameter α_r accounts for the fracturing of the rock. Reese [25] suggests taking $\alpha_r = \frac{1}{3}$ for rock quality designation RQD = 100, and decreasing linearly to RQD = 0. The p–y curve for the plastic range with $y \geq y_a$ and $p \leq p_u$ is given by:

$$p = \frac{p_u}{2} \left(\frac{y}{k_{rm} \, b} \right)^{0.25} \tag{A8}$$
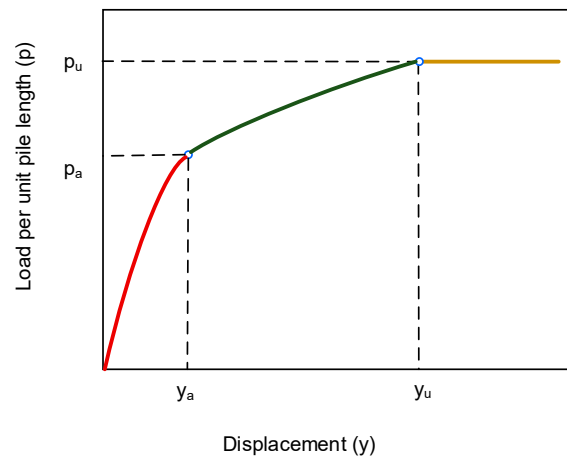
Figure A1. P–Y curve for weak rock, after [65].

Appendix C

This Appendix shows complementary Equations for calculating the geometrical and mechanical properties of dead weight anchors.

Shear keys for DWA

The lateral capacity of this type of anchor with full-base keying skirts in cohesionless soil is computed as:

$$V'_d = (W_{DWA} - V_d) \tan(\phi_s) + K_p \gamma_{soil} \frac{1}{2} Z_s^2 B \tag{A9}$$

The coefficient of lateral earth pressure, K_p, can be defined using the following Equation:

$$K_p = \tan^2 \left(45° + \frac{\phi}{2} \right) \tag{A10}$$

Then, the minimum anchor width/diameter is:

$$B = \left(\frac{6 \, W_{DWA} H_d}{\gamma_c (W_{DWA} - V_d - 0.3 H_d)} \right)^{\frac{1}{3}} \tag{A11}$$

The number of shear keys, n_{sk}, is calculated from:

$$n_{sk} = \left(\frac{200(W_{DWA} - V_d) \, tan(\phi - 5°)}{K_p \gamma_{soil} B^3} \right)^{\frac{1}{3}} \tag{A12}$$

The thickness of the shear keys, t_k, is obtained from:

$$t_k = 0.042 \left(\frac{\gamma_{soil} B^3}{V_d} \right)^{\frac{1}{2}} \tag{A13}$$

The submerged weight of each shear key, W_k, is estimated using the following Equation:

$$W_k = 0.05 \gamma_k B^2 t_k \tag{A14}$$

The embedment force of the shear keys, q_e, can be determined from:

$$q_e = \frac{\gamma_{soil} B^2}{400} \left[20 t_k \, N_q + B \, tan(\phi - 5°) \right] \tag{A15}$$

where γ_k is the specific weight of the anchor shear keys, γ_{soil} is the submerged specific weight of the soil, N_q is the bearing resistance factor, ϕ is the effective angle of internal friction, Z_s is the length of the skirts, and ϕ_s is the friction angle of the soil at depth Z_s.

Effective area of DWA

For a quadratic area, the effective area, A_{eff}, can be defined as:

$$A_{eff} = b_{eff} l_{eff} \tag{A16}$$

where b_{eff}, l_{eff} are the effective dimensions (see Figure A2).
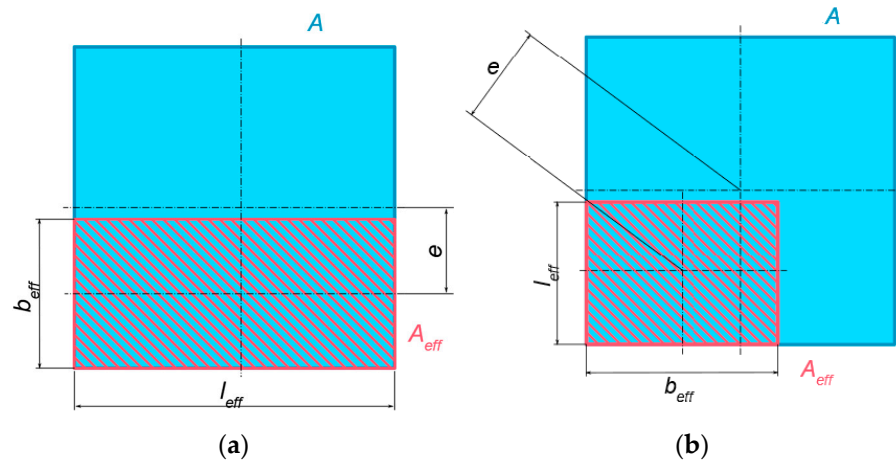
Figure A2. Quadratic footing with two approaches to make up the effective foundation area, based on DNV-OS-J101 [15]. (**a**) Load eccentricity with respect to only one symmetry axis; (**b**) Load eccentricity with respect to both symmetry axes.

Eccentricity with respect to one of the two symmetry axes of the foundation.

In Scenario 1, load eccentricity is determined with respect to only one of the two symmetry axes of the foundation. The effective dimensions are calculated using the following expressions:

$$b_{eff} = B - 2e \tag{A17}$$

$$l_{eff} = B \tag{A18}$$

where e is the eccentricity of the vertical force

Eccentricity with respect to both symmetry axes of the foundation.

Scenario 2. Load eccentricity is determined with respect to both symmetry axes of the foundation. The effective dimensions are calculated using the following expression:

$$b_{eff} = l_{eff} = B - \sqrt{2}e \tag{A19}$$

Circular anchors.

In the case of structures with a circular base, the effective dimensions can be calculated by:
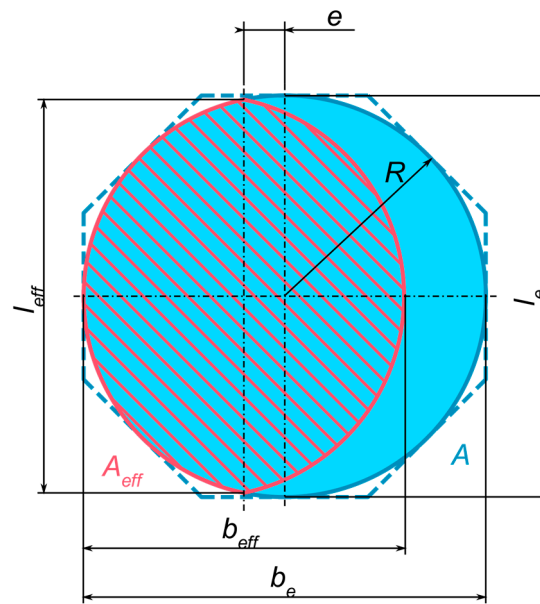
$$b_{eff} = 2\left[\frac{1}{2}B - e\right] \tag{A20}$$

with

$$l_{eff} = B\sqrt{1 - \left[1 - \frac{b_{eff}}{B}\right]^2} \tag{A21}$$

The effective area, A_{eff} (see Figure A3) can be calculated by:

$$A_{eff} = 2\left[\frac{B^2}{4}\arccos\frac{2e}{B} - e\sqrt{\frac{B^2}{4} - e^2}\right] \tag{A22}$$

Figure A3. Circular and octangular footings with the effective foundation area marked out, based on DNV-OS-J101 [15].

Based on the above, A_{eff} can be represented by a rectangle with dimensions b_{eff} and l_{eff}.

$$l_{eff} = \sqrt{A_{eff} \frac{l_e}{b_e}} \tag{A23}$$

$$b_{eff} = \frac{l_{eff}}{l_e} b_e \tag{A24}$$

Additional parameters to calculate bearing capacity in fully drained conditions
Design cohesion

$$c_d = \frac{c}{\gamma_c} \tag{A25}$$

$$\phi_d = atan\left(\frac{tan(\phi)}{\gamma_\phi}\right) \tag{A26}$$

Load factors

$$N_q = \exp(\pi \tan \phi_d)\left[\frac{1 + \sin \phi_d}{1 - \sin \phi_d}\right] \tag{A27}$$

$$N_c = (N_q - 1) \cot \phi_d \tag{A28}$$

$$N_\gamma = \frac{3}{2}(N_q - 1) \tan \phi_d \tag{A29}$$

when bearing capacity formulas are used to predict the reaction forces of the soil on the foundations, the calculation of N_γ should be made using the following Equation:

$$N_\gamma = 2(N_q - 1) \tan \phi_d \tag{A30}$$

Shape factors are defined by the following expressions:

$$s_q = s_c = 1 - 0.2\frac{b_{eff}}{l_{eff}} \tag{A31}$$

$$s_\gamma = 1 - 0.4\frac{b_{eff}}{l_{eff}} \tag{A32}$$

Inclination factors are defined by the following expressions:

$$i_q = i_c = \left[1 - \frac{H_d}{V_d + A_{eff} c_d \cot \phi_d} \right]^2 \tag{A33}$$

$$i_\gamma = i_q^2 \tag{A34}$$

These formulae apply to foundations which are not embedded. However, other formulae may be applied to embedded foundations, which will give conservative results. Alternatively, depth effects associated with embedded foundations can be calculated based on formulae given in DNV-OS-J101 [15].

Additional parameters to calculate bearing capacity for undrained conditions

In the case of undrained conditions, the bearing capacity factors are defined by:

$$N_c^0 = \pi + 2 \tag{A35}$$

$$s_c^0 = s_c \tag{A36}$$

$$i_c^0 = 0.5 + 0.5 \sqrt{1 - \frac{H_d}{A_{eff} \cdot s_{ud}}} \tag{A37}$$

References

1. Astariz, S.; Vazquez, A.; Iglesias, G. Evaluation and comparison of the levelized cost of tidal, wave, and offshore wind energy. *J. Renew. Sustain. Energy* **2015**, *7*, 053112. [CrossRef]
2. Vazquez, A.; Iglesias, G. Capital costs in tidal stream energy projects—A spatial approach. *Energy* **2016**, *107*, 215–226. [CrossRef]
3. Bhattacharya, S. *Design of Foundations for Offshore Wind Turbines*; John Wiley & Sons: Chichester, UK, 2019; Volume 1, ISBN 9788578110796.
4. Starling, M.; Scott, A.; Parkinson, R. *Foundations and Moorings for Tidal Stream Systems*; BMT Cordah Limited: London, UK, 2009.
5. Zhou, Z.; Benbouzid, M.; Charpentier, J.-F.; Scuiller, F.; Tang, T. Developments in large marine current turbine technologies—A review. *Renew. Sustain. Energy Rev.* **2017**, *71*, 852–858. [CrossRef]
6. Meggitt, D.J.; Jackson, E.; Machin, J.; Taylor, R. Marine micropile anchor systems for marine renewable energy applications. In Proceedings of the 2013 MTS/IEEE—San Diego an Ocean Common, San Diego, CA, USA, 23–27 September 2013.
7. Cresswell, N.; Hayman, J.; Kyte, A.; Hunt, A.; Jeffcoate, P. Anchor Installation for the Taut Moored Tidal Platform PLAT-O. In Proceedings of the 3rd Asian Wave Tidal Energy Conference, Singapore, Singapore, 24–28 October 2016; pp. 1–8.
8. Ma, K.-T.; Luo, Y.; Kwan, T.; Wu, Y.B.T. *Mooring System Engineering for Offshore Structures*, 1st ed.; Gulf Professional Publishing: Houston, TX, USA, 2019; ISBN 9780128185513.
9. Hernández-Fontes, J.V.; Felix, A.; Mendoza, E.; Cueto, Y.R.; Silva, R. On the Marine Energy Resources of Mexico. *J. Mar. Sci. Eng.* **2019**, *7*, 191. [CrossRef]
10. Alcérreca-Huerta, J.C.; Encarnacion, J.I.; Ordoñez-Sánchez, S.; Callejas-Jiménez, M.; Barroso, G.G.D.; Allmark, M.; Mariño-Tapia, I.; Casarín, R.S.; O'Doherty, T.; Johnstone, C.; et al. Energy Yield Assessment from Ocean Currents in the Insular Shelf of Cozumel Island. *J. Mar. Sci. Eng.* **2019**, *7*, 147. [CrossRef]
11. Graniel, J.B.; Fontes, J.; Garcia, H.; Silva, R. Assessing Hydrokinetic Energy in the Mexican Caribbean: A Case Study in the Cozumel Channel. *Energies* **2021**, *14*, 4411. [CrossRef]
12. Muckelbauer, G. The shelf of Cozumel, Mexico: Topography and organisms. *Facies* **1990**, *23*, 201–239. [CrossRef]
13. Taylor, R.J. *Interaction of Anchors with Soil and Anchor Design*; Naval Facilities Engineering Command: Port Hueneme, CA, USA, 1982; ISBN 9788578110796.
14. Vanzwieten, J.H.; Seibert, M.G.; Ellenrieder, K. Von Anchor selection study for ocean current turbines. *J. Mar. Eng. Technol.* **2014**, *13*, 59–73. [CrossRef]
15. Det Norske Veritas. *DNV-OS-J101 Design of Offshore Wind Turbine Structures*; Det Norske Veritas: Høvik, Norway, 2014.
16. American Petroleum Institute. *API RP2A-WSD Recommended Practice for Planning, Designing and Constructing Fixed Offshore Platforms—Working Stress Design*; American Petroleum Institute: Washington, DC, USA, 2002.
17. Arany, L.; Bhattacharya, S.; Macdonald, J.; Hogan, S. Design of monopiles for offshore wind turbines in 10 steps. *Soil Dyn. Earthq. Eng.* **2017**, *92*, 126–152. [CrossRef]
18. McCarron, W. *Deepwater Foundations and Pipeline Geomechanics*, 1st ed.; J. Ross Publishing: Fort Lauderdale, FL, USA, 2011; ISBN 9781604270099.
19. Bai, Y.; Jin, W.-L. *Marine Structural Design*, 2nd ed.; Elsevier: Oxford, UK, 2015; ISBN 9780080999975.
20. El-Reedy, M.A. *Marine Structural Design Calculations*, 1st ed.; Butterworth-Heinemann: Oxford, UK, 2015; ISBN 9780080999876.

21. Gaythwaite, J.W. *Design of Marine Facilities*, 3rd ed.; American Society of Civil Engineers: Reston, VA, USA, 2016; ISBN 9780784414309.

22. Fleming, K.; Weltman, A.; Randolph, M.; Elson, K. *Piling Engineering*; CRC Press: London, UK, 2008; ISBN 9780415266468.

23. Ferrero, A.; Migliazza, M.; Roncella, R.; Tebaldi, G. Analysis of the failure mechanisms of a weak rock through photogrammetrical measurements by 2D and 3D visions. *Eng. Fract. Mech.* **2008**, *75*, 652–663. [CrossRef]

24. Dobereiner, L.; De Freitas, M.H. Geotechnical properties of weak sandstones. *Geotechnique* **1986**, *36*, 79–94. [CrossRef]

25. Reese, L.C. Analysis of Laterally Loaded Piles in Weak Rock. *J. Geotechnol. Geoenviron. Eng.* **1997**, *123*, 1010–1017. [CrossRef]

26. Goodman, R.E. *Introduction to Rock Mechanics*, 2nd ed.; John Wiley & Sons: New York, NY, USA, 1980; ISBN 9780471812005.

27. Abbs, A.F. Lateral Pile Analysis in Weak Carbonate Rocks. In Proceedings of the Conference on Geotechnical Practice in Offshore Engineering, Austin, TX, USA, 27–29 April 1983; ASCE: Austin, TX, USA, 1983; pp. 546–556.

28. Carter, J.P.; Kulhawy, F.H. Closure to "Analysis of Laterally Loaded Shafts in Rock" by John P. Carter and Fred H. Kulhawy (June, 1992, Vol. 118, No. 6). *J. Geotechnol. Eng.* **1993**, *119*, 2018–2020. [CrossRef]

29. Gannon, J.A.; Masterton, G.G.T.; Wallace, W.A.; Wood, D.M. *Piled Foundations in Weak Rock*; Construction Industry Research and Information Association (CIRIA): London, UK, 1999.

30. Zhang, L.; Ernst, H.; Einstein, H.H. Nonlinear Analysis of Laterally LoadedRock-Socketed Shafts. *J. Geotechnol. Geoenviron. Eng.* **2000**, *126*, 955–968. [CrossRef]

31. Irvine, J.; Terente, V.; Lee, L.; Comrie, R. Driven pile design in weak rock. In *Frontiers in Offshore Geotechnics III—Proceedings of the 3rd International Symposium on Frontiers in Offshore Geotechnics, Oslo, Norway, 10–12 June 2015*; CRC Press: London, UK, 2015; pp. 569–574. ISBN 9781138028500.

32. International Electrotechnical Commission. *IEC 62600-10 Marine Energy—Wave, Tidal and Other Water (IEC, Current Converters— Part 10: Assessment of Mooring System for Marine Energy Converters)*; International Electrotechnical Commission: Geneva, Switzerland, 2015; ISBN 9782832224311.

33. Das, B.M.; Sivakugan, N. *Principles of Foundation Engineering*, 9th ed.; Cengage Learning, Inc.: Boston, MA, USA, 2019; ISBN 9781337705035.

34. Det Norske Veritas. *DNV-RP-C203 Fatigue Design of Offshore Steel Structures*; Det Norske Veritas: Høvik, Norway, 2014.

35. Det Norske Veritas. *DNV-OS-C502 Offshore Concrete Structures*; Det Norske Veritas: Høvik, Norway, 2010.

36. Poulos, H.G.; Davis, E.H. *Pie Foundation Analysis and Design*; John Wiley and Sons: New York, NY, USA, 1990; ISBN 0894644491.

37. American Institute of Steel Construction (AISC). *LRFD Load and Resistance Factor. Design Specification for Structural Steel Buildings*; American Institute of Steel Construction: Chicago, IL, USA, 1999.

38. Tomlinson, M.; Woodward, J. *Pile Design and Construction Practice*, 6th ed.; CRC Press: Boca Raton, FL, USA, 2015; ISBN 9781466592643.

39. Carrington, T.; Li, G.; Rattley, M. A new assessment of ultimate unit friction for driven piles. In Proceedings of the 15th European Conference on Soil Mechanics and Geotechnical Engineering, Athens, Greece, 12–15 September 2011; Anagnostopoulos, A., Pachakis, M., Tsatsanifos, C., Eds.; IOS Press: Amsterdam, NY, USA, 2011; pp. 825–830.

40. Gabr, M.A.; Borden, R.H.; Cho, K.H.; Clark, S.C.; Nixon, J.B. *P-y Curves for Laterally Loaded Drilled Shafts Embedded in Weathered Rock*; Department of Civil Engineering North Carolina State University: Raleigh, NC, USA, 2002.

41. American Concrete Institute. *ACI 318-08 Building Code Requirements for Structural Concrete and Commentary*; American Concrete Institute: Farmington Hills, MI, USA, 1999; Volume 1, ISBN 9781942727118.

42. Butterfield, R.; Gottardi, G. A complete three-dimensional failure envelope for shallow footings on sand. *Geotechnique* **1994**, *44*, 181–184. [CrossRef]

43. Tistel, J.; Eiksund, G.R.; Hermstad, J.; Bye, A.; Athanasiu, C. Gravity Based Structure foundation design and optimization opportunities. In Proceedings of the Twenty-fifth International Ocean and Polar Engineering Conference, Kailua-Kona, HI, USA, 21–26 June 2015; pp. 772–779.

44. Matlock, H. Correlations for design of laterally loaded piles in soft clay. In Proceedings of the Second Annual Offshore Technology Conference, Houston, TX, USA, 22–24 April 1970.

45. Kallehave, D.; Thilsted, C.L.; Liingaard, M.A. Modification of the API p-y Formulation of Initial Stiffness of Sand. In Proceedings of the Offshore Site Investigation and Geotechnics: Integrated Technologies—Present and Future; Society of Underwater Technology: London, UK, 2012; p. 8.

46. O'Neill, M.W.; Murchison, J.M. *An Evaluation of p-y Relationships in Sands*; Report No. GT-DF02-83; Department of Civil Engineering, University of Houston: Houston, TX, USA, 1983.

47. Winkler, E. *Die Lehre von der Elasticitaet und Festigkeit: Mit besonderer Rucksicht auf ihre Anwendung in der Technik*; H. Dominicus: Prague, Czech Republic, 1868.

48. Wesselink, B.D.; Murff, J.D.; Randolph, M.F.; Nunez, I.L.; Hyden, A.M. *Analysis of Centrifuge Model Test Data from Laterrally Loaded Piles in Calcareous Sand*; CRC Press: London, UK, 1988; pp. 261–270. ISBN 9781003211433.

49. Williams, A.F.; Dunnavant, T.W.; Anderson, S.; Equid, D.W.; Hyden, A.M. The performance and analysis of lateral load tests on 356 mm dia piles in reconstituted calcareous sand. In *Engineering for Calcareous Sediments*; CRC Press: London, UK, 1988; pp. 271–280. ISBN 9781003211433.

50. Dyson, G.J.; Randolph, M.F. Monotonic lateral loading of piles in calcareous sand. *J. Geotechnol. Geoenviron. Eng.* **2001**, *127*, 346–352. [CrossRef]

51. Fragio, A.G.; Santiago, J.L.; Sutton, V.J.R. Load tests on grouted piles in rock. In Proceedings of the Annual Offshore Technology Conference, Houston, TX, USA, 6–9 May 1985; pp. 93–104.

52. Turner, J. *Rock-Socketed Shafts for Highway Structure Foundations*, 1st ed.; Transportation Research Board of the National Academies: Laramie, WY, USA, 2006.

53. Liang, R.; Yang, K.; Nusairat, J. p-y Criterion for Rock Mass. *J. Geotechnol. Geoenviron. Eng.* **2009**, *135*, 26–36. [CrossRef]

54. Zdravkovic, L.; Taborda, D.; Potts, D.; Jardine, R.; Sideri, M.; Schroeder, F.; Byrne, B.; McAdam, R.; Burd, H.; Houlsby, G.; et al. Numerical modelling of large diameter piles under lateral loading for offshore wind applications. In *Frontiers in Offshore Geotechnics III—Proceedings of the 3rd International Symposium on Frontiers in Offshore Geotechnics, Oslo, Norway, 10–12 June 2015*; CRC Press: London, UK, 2015; pp. 569–574. ISBN 9781138028500. [CrossRef]

55. Byrne, B.; Mcadam, R.; Burd, H.; Houlsby, G.; Martin, C.; Gavin, K.; Doherty, P.; Igoe, D.; Taborda, D.M.G.; Potts, D.; et al. Field testing of large diameter piles under lateral loading for offshore wind applications Field testing of large diameter piles under lateral loading for offshore wind applications. In Proceedings of the XVI ECSMGE Geotechnical Engineering for Infrastructure and Development, Edinburgh, UK, 13–17 September 2015; pp. 1255–1260.

56. Ashour, M.; Norris, G.; Pilling, P. Lateral Loading of a Pile in Layered Soil Using the Strain Wedge Model. *J. Geotechnol. Geoenviron. Eng.* **1998**, *124*, 303–315. [CrossRef]

57. Det Norske Veritas. *DNV GL-ST-0126 Support Structures for Wind Turbines*; Det Norske Veritas: Høvik, Norway, 2016.

58. Harris, C.R.; Millman, K.J.; van der Walt, S.J.; Gommers, R.; Virtanen, P.; Cournapeau, D.; Wieser, E.; Taylor, J.; Berg, S.; Smith, N.J.; et al. Array programming with NumPy. *Nature* **2020**, *585*, 357–362. [CrossRef] [PubMed]

59. International Electrotechnical Commission. *IEC 62600-2 Marine Energy—Wave, Tidal and Other Water Current Converters—Part 2: Design Requirements for Marine Energy Systems*; International Electrotechnical Commission: Geneva, Switzerland, 2016; ISBN 9782832235805.

60. Dynamic Systems Analysis ProteusDS Manual v2.29.2. 2016. Available online: https://dsaocean.com/downloads/documentation/ProteusDS2015Manual.pdf. (accessed on 1 July 2021).

61. Dhanak, M.R.; Xiros, N.I. *Springer Handbook of Ocean Engineering*; Springer: Trento, Italy, 2016; ISBN 9783319166490.

62. Betz, A. Das Maximum der Theoretisch Möglichen Ausnutzung des Windes durch Windmotoren. In *Zeitschrift für das Gesamte Turbinenwes*; R. Oldenbourg: Munich, Germany, 1920; p. 20.

63. Clarke, J.; Grant, A.; Connor, G.; Johnstone, C. Development and in-sea performance testing of a single point mooring supported contra-rotating tidal turbine. In Proceedings of the International Conference on Offshore Mechanics and Arctic Engineering—OMAE, Honolulu, Hawaii, USA, 31 May–5 June 2009; Volume 4, pp. 1065–1073.

64. Ivashov, A. SMath Studio (Versión 0.99.7030). Available online: https://en.smath.com/view/SMathStudio/summary (accessed on 1 July 2021).

65. Doherty, J.P. Lateral Analysis of Piles User Manual v 2.0. 2020. Available online: www.geocalcs.com/lap. (accessed on 1 July 2021).